ORGANOMETALLICS

Article

pubs.acs.org/Organometallics

Synthesis and Hydrolysis of Uranyl, Neptunyl, and Plutonyl Gas-Phase Complexes Exhibiting Discrete Actinide−Carbon Bonds

Phuong D. Dau,[†] Daniel Rios,[†] Yu Gong,[†] Maria C. Michelini,[*,‡] Joaquim Marçalo,[§] David K. Shuh,[†] Mejdi Mogannam,[∥] Michael J. Van Stipdonk,[⊥] Theodore A. Corcovilos,[#] Jonathan K. Martens,[▽] Giel Berden,[▽] Jos Oomens,[▽,○] Britta Redlich,[▽] and John K. Gibson[*,†]

[†]Chemical Sciences Division, Lawrence Berkeley National Laboratory, Berkeley, California 94720, United States

[‡]Dipartimento di Chimica, Università della Calabria, 87030 Arcavacata di Rende, Italy

[§]Centro de Ciências e Tecnologias Nucleares, Instituto Superior Técnico, Universidade de Lisboa, 2695-066 Bobadela LRS, Portugal

[∥]Skyline College, San Bruno, California 94066, United States

[⊥]Department of Chemistry and Biochemistry, Duquesne University, Pittsburgh, Pennsylvania 15282, United States

[#]Department of Physics, Duquesne University, Pittsburgh, Pennsylvania 15282, United States

[▽]Radboud University, Institute for Molecules and Materials, FELIX Laboratory, Toernooiveld 7c, 6525ED Nijmegen, The Netherlands

[○]van 't Hoff Institute for Molecular Sciences, University of Amsterdam, Science Park 904, 1098XH Amsterdam, The Netherlands

Supporting Information

ABSTRACT: Gas-phase organoactinyl complexes possessing discrete An−C bonds (An = U, Np, Pu) were synthesized in a quadrupole ion trap by endothermic decarboxylation of $[AnO_2(O_2C{-}R)_3]^-$ anion complexes in which a formally AnO_2^{2+} actinyl core is coordinated by three carboxylate ligands, with R = CH_3 (methyl), CH_3CC (1-propynyl), C_6H_5 (phenyl), C_6F_5 (pentafluorophenyl). Decarboxylation and competing ligand loss were studied computationally by density functional theory complementing experiment. Although decarboxylation was computed to be the energetically most favorable process in all cases, reduction from An(VI) to An(V) via neutral ligand loss was often prevalent, particularly for An = Np, Pu, presumably resulting from barriers associated with decarboxylation. Comparative hydrolysis rates of the An−C bonds were experimentally determined, and the chemical properties of these bonds were analyzed by the quantum theory of atoms in molecules. The measured hydrolysis rates differed by up to 3 orders of magnitude: the fastest was for $[(CH_3CC)UO_2(O_2C{-}CCCH_3)_2]^-$ and the slowest for $[(C_6F_5)PuO_2(O_2C{-}C_6F_5)_2]^-$. There is a general correlation between hydrolysis exothermicity and hydrolysis rate. Prototypical hydrolysis reaction pathways computed for R = CH_3 (An = U, Np) reveal a mechanism in which an outer-sphere water becomes inner-sphere concomitant with transfer of an H atom to yield an OH ligand and CH_4, with a net energy release of 170 kJ mol^{-1} and a transition state barrier of 45 kJ mol^{-1} for An = U. Infrared multiphoton dissociation spectra of selected complexes were acquired to confirm the predicted structures by agreement between the computed and observed vibrational frequencies. The experiment and theory results provide an evaluation of the comparative propensities for formation of the organoactinyls as a function of actinide and carboxylate and an assessment of the nature and stability toward hydrolysis of the primarily ionic An−C bonds.

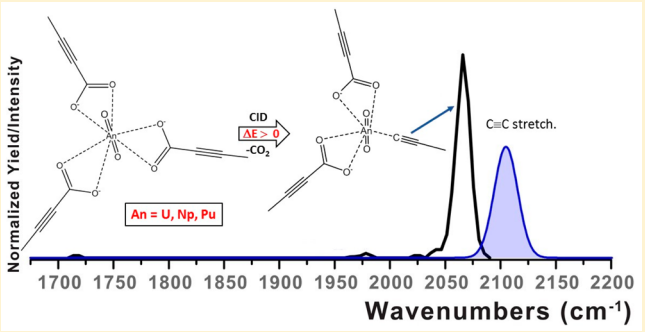

INTRODUCTION

Although the first organouranium compounds were first mentioned in the literature as early as the mid-1800s,[1] organoactinide chemistry only took off in 1956 with the preparation of cyclopentadienyl compounds of uranium by Reynolds and Wilkinson.[1,2] The synthesis, structure, and bonding of bis(cyclooctatetraenyl)uranium (uranocene) was first reported in a seminal paper by Streitwieser and Müller-Westerhoff in 1968.[3] The focuses of the present work are the distinctive linear hexavalent actinyl ions $[O{=}An{=}O]^{2+}$ (An = U, Np, Pu), which exist in solutions and as solids. Uranyl is particularly ubiquitous, with plutonyl being less common than Pu(IV) and neptunyl(VI) being rare relative to $Np^{V}O_2^{+}$.[4,5] In view of the particular importance of uranyl, the synthesis of organouranyl complexes has been a longstanding goal. Although the organometallic chemistry of the uranyl ion is relatively underdeveloped, significant success has recently been

Received: January 29, 2016
Published: April 27, 2016

DOI: 10.1021/acs.organomet.6b00079
Organometallics 2016, 35, 1228−1240

achieved in the formation of organometallic uranyl complexes, as well as other organouranium complexes containing uranium−carbon σ bonds.[6,7] Among the reported organouranyl compounds are chelate complexes in which the U−C bond is stabilized by a superstructure involving interactions with other atoms in the ligand.[8−12] Hayton and co-workers prepared the first genuine uranyl(VI)−alkyl complex.[13] Ephritikhine and co-workers prepared the first cyclopentadienyl complex of uranyl[14] and subsequently also complexes containing U−C single and double bonds in chelate complexes.[10] Despite extensive studies of neptunyl and plutonyl chemistry,[5] to the best of our knowledge there have been no reports of neptunyl or plutonyl complexes containing actinide−carbon bonds. The central goal of the present work is to expand the chemistry of uranyl with discrete U−C bonds and, more distinctively, to prepare neptunyl and plutonyl complexes comprising discrete Np−C and Pu−C bonds. A further goal is to characterize these complexes experimentally, by studying their reactivity (hydrolysis) and infrared spectra, and computationally, by evaluating their geometries and bonding characteristics.

Decarboxylation reactions of condensed-phase metal carboxylates is a well-established method of synthesis of organometallic compounds.[15−17] Deacon and collaborators have synthesized and studied the structural and vibrational properties of uranyl pentafluorobenzoate and its coordination derivatives with 2,2′-bipyridyl, triphenylphosphine oxide, and triphenylarsine oxide. This report includes thermal decomposition studies of the same solution complexes, which however do not yield $UO_2(C_6F_5)_2$ derivatives by decarboxylation.[16]

The formation of metal−carbon bonds can be induced in gas-phase ion complexes by collision-induced dissociation (CID) in an ion trap.[18−21] The following reaction was observed for the particular case of alkaline-earth-metal acetates (M = Mg, Ca, Sr, Ba):[19] $[M(O_2C{-}CH_3)_3]^- \rightarrow [(CH_3)M(O_2C{-}CH_3)_2]^- + CO_2$. O'Hair and co-workers have additionally produced and characterized a variety of other gas-phase complexes containing metal−carbon bonds by CID decarboxylation.[20,22−28] Although most of the metal−carbon bonds produced were for group 11 transition metals, their success in producing metal−carbon bonds for the highly electropositive alkaline-earth metals suggests that it should be feasible to similarly prepare actinyl complexes containing discrete actinide−carbon bonds by CID of carboxylate anion complexes, $[AnO_2(O_2C{-}R)_3]^-$, where R is an organic radical (CH_3 in the case of acetate).

It has been long known that organoactinide complexes are unstable in aqueous solution and undergo rapid hydrolysis.[1,4] O'Hair and co-workers have demonstrated that relative rates of hydrolysis of Mg−C bonds in gas-phase complexes reflect the inherent stabilities of the organomagnesium bonds,[26] suggesting gas-phase hydrolysis as an approach to similarly assess the susceptibility toward the hydrolysis of An−C bonds.

Reported here are the syntheses, by decarboxylation, of actinyl complexes with direct An−C bonds for An = U, Np, Pu. Gas-phase reactions with water were employed to evaluate the comparative susceptibilities of the An−C bonds toward hydrolysis for the three actinides as well as for different organic ligands. The observations, including variations in decarboxylation and hydrolysis efficiencies for different carboxylate ligands and differences between the three actinyls, have been elucidated by density functional theory (DFT) computations. The An−C bond properties were analyzed by quantum theory of atoms in molecules (QTAIM). Infrared multiphoton dissociation (IRMPD) of molecular ions has been shown to be a powerful technique to characterize organometallic ions in the gas phase.[29] IRMPD spectra were acquired for selected complexes to confirm the computed structures and bonding.

EXPERIMENTAL SECTION

Caution! The ^{238}U, ^{237}Np, and ^{242}Pu isotopes used in this work are α-emitting radionuclides. Special safety precautions must be followed when handling them.

General Considerations. The following stock acid solutions were used to prepare the actinyl carboxylate complexes used for electrospray ionization (ESI): 177 mM $U^{VI}O_2(ClO_4)_2$ at pH 0.6, 0.83 mM $Np^{VI}O_2(ClO_4)_2$ at pH 1.6, 0.70 mM $Pu^{VI}O_2(ClO_4)_2$ at pH 1.6, and 80 mM carboxylate. The ESI solutions were acetone and water (<25% H_2O) with the following actinyl:carboxylate concentrations in mM: uranyl, 0.18:1.4; neptunyl, 0.17:1.4; plutonyl, 0.14:1.4. The ESI mass spectrometry experiments were performed using an Agilent 6340 quadrupole ion trap mass spectrometer (QIT/MS) with MS^n collision-induced dissociation (CID) capabilities. Additionally, ions in the trap can undergo ion−molecule reactions for a fixed time at ∼300 K.[30] The source region of the QIT/MS is inside of a radiological-containment glovebox, as described in detail elsewhere.[31] In high-resolution mode, the instrument has a detection range of m/z 50−2200 and a resolution of m/z ∼0.3 fwhm measured at m/z 500 (i.e., a resolution of ∼1600). Mass spectra were acquired using the following instrumental parameters: solution flow rate, 60 μL min^{-1}; nebulizer gas pressure, 12 psi; capillary voltage and current, −4000 V and 100 nA; end plate voltage offset and current, −500 V and 450 nA; dry gas flow rate, 3 L/min; dry gas temperature, 325 °C; capillary exit, −50.0 V; skimmer, −36.3 V; octopole 1 and 2 dc, −10.88 and −3.00 V; octopole RF amplitude, 190.0 V_{pp}; lens 1 and 2, −10.0 and 91.0 V; trap drive, 50.0. High-purity nitrogen gas for nebulization and drying in the ion transfer capillary was supplied from the boil-off of a liquid nitrogen Dewar. As has been discussed elsewhere,[32] the background water pressure in the ion trap is estimated as $\sim 10^{-6}$ Torr; the reproducibility of hydration rates of $UO_2(OH)^+$ [33] confirms that the background water pressure in the trap varies by less than ±50%. The helium buffer gas pressure in the trap is constant at $\sim 10^{-4}$ Torr.

The CID decarboxylation products $[(R)AnO_2(O_2C{-}R)_2]^-$ were isolated in the ion trap to study the kinetics of hydrolysis with background water. The linear decay of the logarithm of the reactant ion intensity as a function of time reveals pseudo-first-order kinetics, for which rates were determined from the slopes of the decay plots.[31] The measured kinetics were normalized to an arbitrary typical background water pressure by determining variations (<50%) in water pressure from the rate of hydration of $UO_2(OH)^+$.[33−35] Although the use of a background gas is generally not ideal for measuring ion−molecule reaction kinetics, the ability here to rather accurately (to within <10%) measure the relative water pressure for each experiment, and thereby normalize the measured kinetics, enables making reliable comparisons. Each reported rate is the average of at least three different experiments. Representative kinetics results are included in the Supporting Information.

The IRMPD experiments were limited to uranyl complexes due to the much greater radiological hazards presented by neptunyl and plutonyl, which precludes gas-phase spectroscopic studies of the last two species at the Free Electron Laser for Infrared eXperiments (FELIX) laboratory.[36] The studied uranyl complexes were produced by ESI in a manner similar to that described above, and the IRMPD spectra were acquired using a QIT/MS instrument similar to that employed for the reactivity studies. CID of uranyl carboxylate complexes was performed as described above to obtain organouranyl complexes. Hydrolysis in the ion trap produced hydroxides for spectroscopic studies. The QIT/MS has been modified[37] such that the high-intensity tunable IR beam from FELIX can be directed into the ion packet, resulting in multiphoton dissociation that is appreciable only when the IR frequency is in resonance with an adequately high absorption vibrational mode of the particular mass-selected complex being studied. The FEL produces ∼5 μs long IR pulses with an energy of typically 40 mJ, which are in the form of a sequence of ∼1 ps long

DOI: 10.1021/acs.organomet.6b00079
Organometallics 2016, 35, 1228−1240

micropulse at a 1 GHz repetition rate. The wavelength of the radiation was tuned between 4.9 and 15 μm in these experiments.

Computational Details. DFT was used to compute $[UO_2(O_2C{-}R)_3]^-$ decarboxylation energies as well as possible competitive reaction energies (i.e., ligand elimination) for R = CH_3 (methyl), CH_3CC (1-propynyl), C_6H_5 (phenyl), C_6F_5 (pentafluorophenyl). Geometry optimizations and frequency calculations were initially performed using the local exchange and correlation functional (local density approximation, LDA) together with the small core Stuttgart−Dresden relativistic effective core potential (ECP60MWB) and the [8s7p6d4f] associated orbital basis sets for uranium (referred to as SDD in Gaussian09),[38,39] whereas extended double-ζ (DZ) basis sets (6-31G*) were used for the rest of the atoms (LDA/DZ hereafter). Previous computational studies have shown that the local density functional and the SDD basis sets produce reliable optimized geometrical structures and frequencies for systems containing uranium.[40−42] Single-point calculations were performed on all the optimized isomers of each species using the B3LYP hybrid functional,[43,44] the same basis sets for the actinide element (SDD), and the extended triple-ζ (TZ) basis sets 6-311++G** for the rest of the atoms (B3LYP/TZ//LDA/DZ hereafter). Calculations were performed using the NWCHEM 6.1[45] and Gaussian09 (rev. B.01)[46] codes. The lowest-energy isomers of each species were used to compute the reaction energies, which in all cases include the zero-point energy corrections at 0 K (ΔE°). To further test the validity of the approach, the reactions involving the acetate ligand were reoptimized at the B3LYP/SDD(U):6-311++G** (B3LYP/TZ) level, and the new set of results was compared with the B3LYP/TZ//LDA/DZ results. The reaction energies were not significantly affected by an increase in the quality of the basis sets or by the use of the B3LYP functional for the geometry optimization of the structures; the largest observed energy change was 7 kJ mol^{-1}. Therefore, the rest of the dissociation reaction energies involving uranyl were obtained at the B3LYP/TZ//LDA/DZ level of theory. In selected cases the computational study was extended to neptunyl and plutonyl, to analyze the trend of properties along the series from U to Np to Pu. In particular, the dissociation reactions were also computed for $[PuO_2(O_2C{-}R)_3]^-$ (R = CH_3, CH_3CC). A comparison of the results obtained at the B3LYP/TZ//LDA/DZ level with those in which the geometry optimization was directly performed at the B3LYP/TZ level for $[PuO_2(O_2C{-}CH_3)_3]^-$ indicates a greater departure in the obtained dissociation energies at the different levels (up to 31 kJ mol^{-1}) with respect to the same comparison for uranyl.

The hydrolysis energetics of all the experimentally observed $[(R)AnO_2(O_2C{-}R)_2]^-$ complexes were also computed. A goal of these computations was to provide insights into the susceptibility toward hydrolysis of the organoactinyl bonds and the relative rate trends observed experimentally along the uranyl/neptunyl/plutonyl series. Given the small changes in the hydrolysis energies on comparison of different actinides for a given ligand and the larger discrepancy found between B3LYP/TZ//LDA/DZ and the B3LYP/TZ levels for the $[PuO_2(O_2C{-}CH_3)_3]^-$ dissociation energies, only the more accurate B3LYP/TZ results are reported for the hydrolysis reactions. Although a thorough evaluation of the hydrolysis mechanisms is beyond the scope of this study, a preliminary analysis of the mechanism was obtained at the B3LYP/TZ level of theory for the smallest ligand (R = CH_3) and An = U, Np. The reported transition states have been checked by analysis of the vibrational mode involving an imaginary frequency and further confirmed using the intrinsic reaction mechanism approach (IRC).[47−49]

QTAIM bonding analysis[50] was performed on the $[AnO_2(O_2C{-}R)_3]^-$ parent complexes, as well as on all the studied decarboxylation and hydrolysis products. Appropriate wave function extended files (wfx) were obtained at the B3LYP/TZ level of theory using Gaussian09 (rev. B.01)[46] and analyzed using the AIMAll package.[51] A short description of the QTAIM approach and of the properties used to analyze the bonding characteristics is provided as Supporting Information.

RESULTS AND DISCUSSION

Decarboxylation of $[AnO_2(O_2C{-}R)_3]^-$ by Collision-Induced Dissociation. CID spectra for $[AnO_2(O_2C{-}R)_3]^-$ complex ions are shown in Figures 1 and 2 for R = CH_3, CH_3CC, respectively; CID spectra for R = C_6H_5, C_6F_5 are given in Figures S1 and S2 in the Supporting Information, and a summary of the CID results is given in Table 1. Three possible CID pathways are given by eq 1 (decarboxylation), eq 2 (anion ligand loss), and eq 3 (neutral ligand loss). Due to the fixed low-mass cutoff of the QIT/MS (27% of the precursor ion

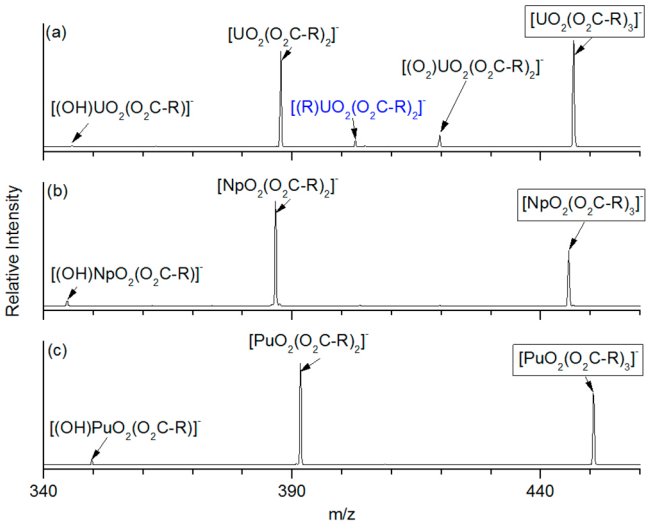

Figure 1. CID spectra of $[AnO_2(O_2C{-}R)_3]^-$ for R = CH_3: (a) An = U; (b) An = Np; (c) An = Pu. Neutral ligand loss with reduction of An^{VI} to An^{V} occurs in all cases. The decarboxylation product (in blue) is apparent only for $[UO_2(O_2C{-}CH_3)_3]^-$, the minor hydrolysis product is apparent for all three, and O_2 addition occurs only for the U^V product.

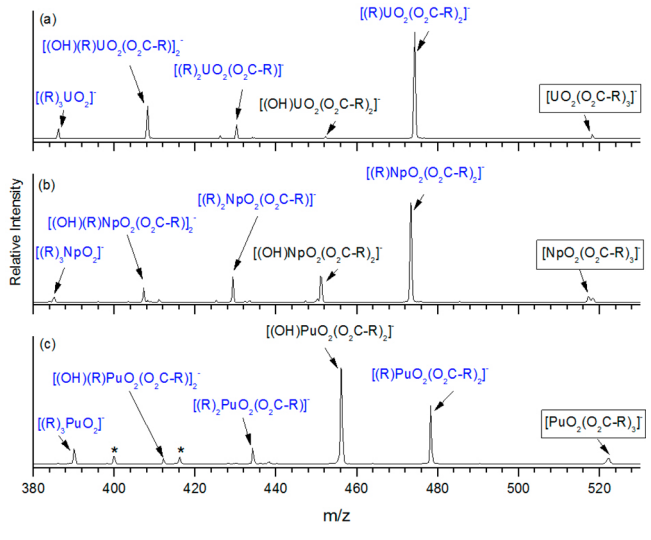

Figure 2. CID spectra of $[AnO_2(O_2C{-}R)_3]^-$ for R = CH_3CC: (a) An = U; (b) An = Np; (c) An = Pu. Decarboxylation is apparent for all three complexes, producing the organoactinyl complexes $[(CH_3CC)_mAnO_2(O_2C{-}CCCH_3)_{3-m}]^-$ (m = 1−3). Hydrolysis is also apparent. Peaks labeled by asterisks in (c) are likely due to impurities in the parent CID peak, which is primarily $[PuO_2(O_2C{-}CCCH_3)_3]^-$.

DOI: 10.1021/acs.organomet.6b00079
Organometallics 2016, 35, 1228−1240

Table 1. Primary Product Distributions for CID of $[An^{VI}O_2(O_2C{-}R)_3]^-$ [a]

	decarboxylation (eq 1)			neutral ligand loss (eq 3)		
R[b]	U	Np	Pu	U[c]	Np	Pu
CH_3	vw	–	–	vs	vs	vs
C_6H_5	w	–	–	vs	vs	vs
C_6F_5[d]	s	s	s	–	vw	–
CH_3CC	vs	vs	m[e]	–	–	–

[a]Yields relative to all observed products: very strong (vs), ≥70%; strong (s), 40–70%; medium (m), 20–40%; weak (w), 10–20%; very weak (vw) ≤10%; not observed (–), < 1%. [b]A CID voltage of 0.7 V was necessary to induce decarboxylation for R = CH_3, C_6H_5; a voltage of 0.4 V was adequate for R = C_6F_5, $CCCH_3$. [c]Includes $[(O_2)UO_2(O_2C{-}R)_2]^-$ (eq 4). [d]Fluoride products $[(F)AnO_2(O_2C{-}R)]^-$ are also observed for U (s), Np (m), and Pu (m). [e]For Pu, the dominant product is $[(OH)PuO_2(O_2C{-}R)_2]^-$ (vs).

mass), the product of CID eq 2 would not have been detected in the experiments. CID of $[AnO_2(O_2C{-}CH_3)_3]^-$ (Figure 1) produced detectable (ca. 5%) $[(CH_3)AnO_2(O_2C{-}CH_3)_2]^-$ (eq 1) only for An = U; for all three An species, the dominant observed CID channel was neutral ligand loss to produce $[AnO_2(O_2C{-}CH_3)_2]^-$ with reduction from An^{VI} to An^V (eq 3). The minor distinctive O_2-addition product $[(O_2)UO_2(O_2C{-}CH_3)_2]^-$ is attributed to oxidation of U^V to U^{VI} by formation of a superoxide complex, as discussed previously (eq 4).[33,40,52–55] A potential alternative source of $[(O_2)UO_2(O_2C{-}CH_3)_2]^-$ would be CID elimination of C–CH_3 from $[UO_2(O_2C{-}CH_3)_3]^-$. Although this CID process cannot be excluded, it was previously demonstrated that eq 4 occurs spontaneously and efficiently for $[UO_2(O_2C{-}CH_3)_2]^-$ by reaction with background oxygen in the ion trap under essentially the same experimental conditions as were employed in the present work.[55] The minor $[(OH)An^VO_2(O_2C{-}CH_3)]^-$ products are attributed to hydrolysis by reaction with background water in the ion trap; it is feasible, but uncertain, that the hydroxides result from hydrolysis of $[(CH_3)AnO_2(O_2C{-}CH_3)]^-$, as discussed below. CID spectra for $[AnO_2(O_2C{-}C_6H_5)_3]^-$ (Figure S1) also exhibit primarily ligand loss to yield $[AnO_2(O_2C{-}C_6H_5)_2]^-$, with decarboxylation apparent only for An = U to yield the minor product $[(C_6H_5)UO_2(O_2C{-}C_6H_5)_2]^-$.

$$[An^{VI}O_2(O_2C{-}R)_3]^- \rightarrow [(R)An^{VI}O_2(O_2C{-}R)_2]^- + CO_2 \quad (1)$$

$$[An^{VI}O_2(O_2C{-}R)_3]^- \rightarrow [An^{VI}O_2(O_2C{-}R)_2] + [RCO_2]^- \quad (2)$$

$$[An^{VI}O_2(O_2C{-}R)_3]^- \rightarrow [An^{V}O_2(O_2C{-}R)_2]^- + R^{\bullet} + CO_2 \quad (3)$$

$$[U^{V}O_2(O_2C{-}R)_2]^- + O_2 \rightarrow [(O_2)U^{VI}O_2(O_2C{-}R)_2]^- \quad (4)$$

In contrast to $[AnO_2(O_2C{-}CH_3)_3]^-$ and $[AnO_2(O_2C{-}C_6H_5)_3]^-$, a dominant CID pathway for $[AnO_2(O_2C{-}$

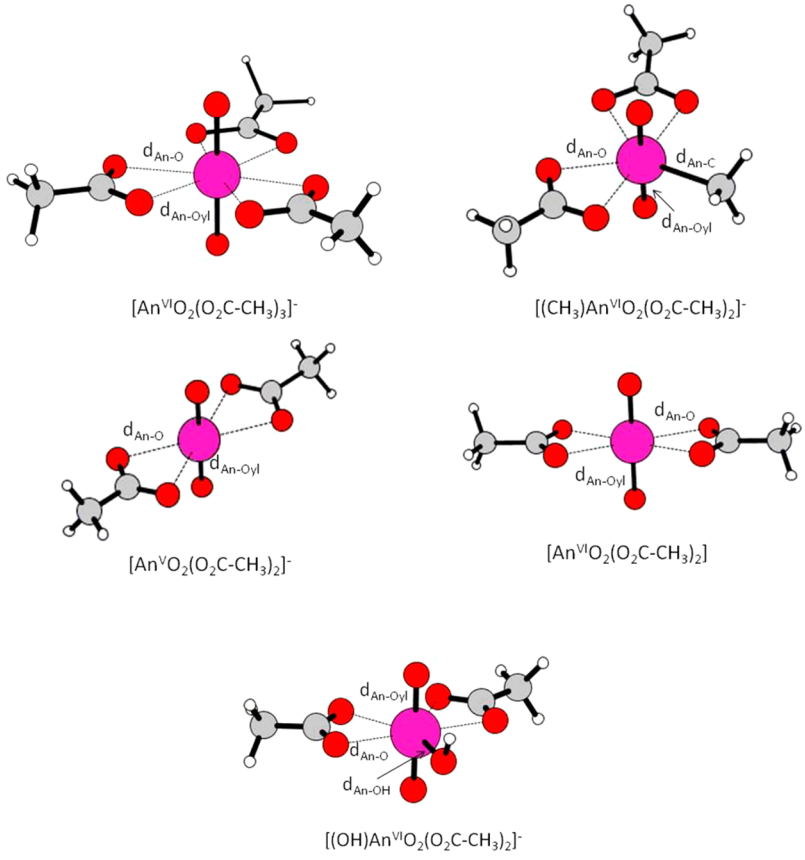

Figure 3. $[AnO_2(O_2C{-}CH_3)_3]^-$, $[(CH_3)AnO_2(O_2C{-}CH_3)_2]^-$, $[AnO_2(O_2C{-}CH_3)_2]^-$, $[AnO_2(O_2C{-}CH_3)_2]$, and $[(OH)AnO_2(O_2C{-}CH_3)_2]^-$ ground-state geometrical structures. Selected geometrical parameters for these species and similar structures for all of the studied ligands are reported in Tables S1–S4 in the Supporting Information.

DOI: 10.1021/acs.organomet.6b00079
Organometallics 2016, 35, 1228–1240

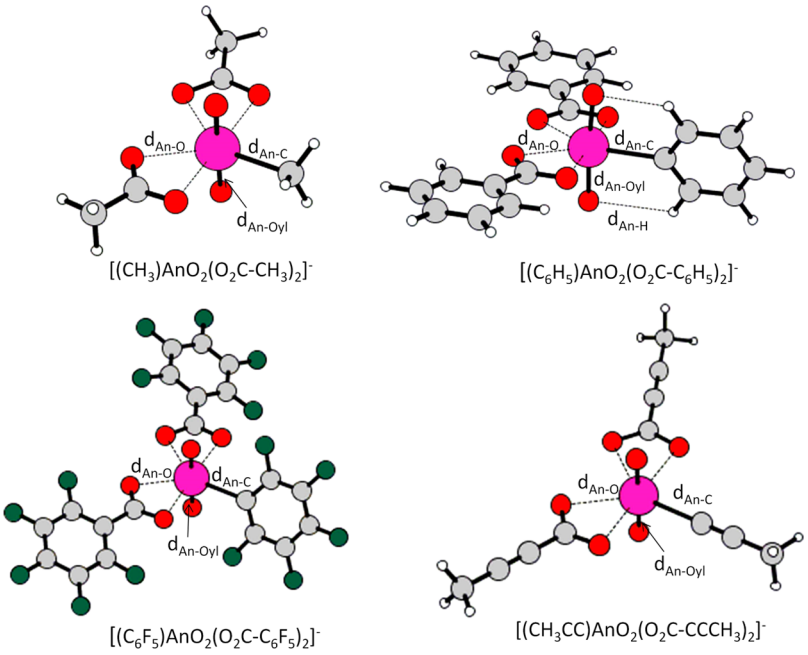

Figure 4. Decarboxylation product $[(R)AnO_2(O_2C{-}R)_2]^-$ ground-state geometrical structures, R = CH_3, C_6H_5, C_6F_5, CH_3CC. Selected geometrical parameters are reported in Table S1 in the Supporting Information.

Table 2. Computed Decarboxylation (Eq 1) and Ligand Loss (Eqs 2 and 3) Energies, $\Delta E°$, for R = CH_3, CH_3CC (Uranyl and Plutonyl) and R = C_6H_5, C_6F_5 (Uranyl) [a]

	$\Delta E°$(eq 1)		$\Delta E°$(eq 2)		$\Delta E°$(eq 3)	
R	U	Pu	U	Pu	U	Pu
CH_3	150 [152]	128 [97]	235 [241]	234 [217]	263 [250]	115 [101]
C_6H_5	160		226		332	
C_6F_5	65		213		226	
CH_3CC	80	[23]	218	[190]	218	[31]

[a] In kJ mol^{-1}, obtained at the B3LYP/TZ//LDA/DZ level of theory; B3LYP/TZ results are given in brackets.

$CCCH_3)_3]^-$ was decarboxylation to yield $[(CH_3CC)$-$AnO_2(O_2C{-}CCCH_3)_2]^-$ for all three An (Figure 2); elimination of one and two additional CO_2 molecules produced $[(CH_3CC)_2AnO_2(O_2C{-}CCCH_3)]^-$ and $[(CH_3CC)_3AnO_2]^-$, respectively. Hydrolysis products are also apparent in the CID spectra, with $[(OH)PuO_2(O_2C{-}CCCH_3)_2]^-$ being particularly abundant. As discussed below, among the three $[(CH_3CC)$-$AnO_2(O_2C{-}CCCH_3)_2]^-$ species, that with An = Pu was the least susceptible to spontaneous exothermic hydrolysis. The high abundance of $[(OH)PuO_2(O_2C{-}CCCH_3)_2]^-$ in the CID spectrum suggests either a hyperthermal process or an entirely different hydrolysis pathway.

CID of $[AnO_2(O_2C{-}C_6F_5)_3]^-$ (An = U, Np, Pu) also resulted in substantial elimination of one or two CO_2 molecules to yield abundant $[(C_6F_5)AnO_2(O_2C{-}C_6F_5)_2]^-$ and $[(C_6F_5)_2AnO_2(O_2C{-}C_6F_5)]^-$ (Figure S2 in the Supporting Information); the yields of $[(C_6F_5)_3AnO_2]^-$ were minor. For all three An species, F atom transfer was also prevalent, producing $[(F)AnO_2(O_2C{-}C_6F_5)_2]^-$ and $[(F)(C_6F_5)AnO_2(O_2C{-}C_6F_5)]^-$. Similar halogen atom transfer was recently reported for actinyls coordinated by halogenated acetates.[56]

Computed Dissociations of $[AnO_2(O_2C{-}R)_3]^-$. A goal of the computations was to evaluate the origins of the $[AnO_2(O_2C{-}R)_3]^-$ product abundances observed during CID, particularly whether the distributions were determined by thermodynamics or by kinetics. Another objective was to analyze the geometrical structures and bonding of the decarboxylation products to corroborate that the lowest-energy isomers correspond to organometallic compounds: i.e., that the $[(R)AnO_2(O_2C{-}R)_2]^-$ ground-state (GS) structures have discrete An−C bonds. With these goals, geometry optimizations and frequency calculations were performed as indicated in Computational Details, and the reaction energies for the decarboxylation process (eq 1), as well as anion and neutral ligand loss (eqs 2 and 3, respectively), were computed for R = CH_3, C_6H_5, C_6F_5, CH_3CC and for An = U. Representative GS structures for R = CH_3 are shown in Figure 3; selected optimized geometrical parameters for the species involved in all the studied reactions are reported in Tables S1−S4 in the Supporting Information. Schematic geometrical structures of the $[(R)AnO_2(O_2C{-}R)_2]^-$ ground-state decarboxylation products are shown in Figure 4, and the corresponding geometrical parameters are reported in Table S1.

Considering the similarities observed between the $[AnO_2(O_2C{-}CH_3)_3]^-$ and $[(AnO_2(O_2C{-}C_6H_5)_3]^-$ CID spectra, as well as between those for $[AnO_2(O_2C{-}CCCH_3)_3]^-$ and $[AnO_2(O_2C{-}C_6F_5)_3]^-$, the influence of the actinide atom on the reaction energetics was only analyzed for two representative ligands, $[O_2C{-}CH_3]^-$ and $[O_2C{-}CCCH_3]^-$, and two representative actinides, U and Pu. The results are summarized in Table 2. In the case of the neutral ligand elimination, the most stable products involve dissocia-

DOI: 10.1021/acs.organomet.6b00079
Organometallics 2016, 35, 1228−1240

tion of the ligand into $R^{\bullet}$ + CO_2 (eq 3), this being in contrast to the lowest-energy pathway for the loss of the intact anionic $[O_2C{-}R]^-$ ligand (eq 2). The thermodynamic instability of neutral carboxyl radicals, which easily lose carbon dioxide to produce the corresponding alkyl radicals, is known; previous experimental studies have shown that this dissociation occurs.[57]

The optimized geometrical parameters of the $[An^{VI}O_2(O_2C{-}R)_3]^-$ precursor ions are reported in Table S2 in the Supporting Information, together with the QTAIM properties of the An−O_{yl} bond. The GS structures of these ions display equatorial coordination number 6 in the case of uranyl (shown for R = CH_3 in Figure 3), followed close in energy by pentacoordinate isomers containing one monodentate carboxylate ligand. At the B3LYP/TZ level of theory, $[U^{VI}O_2(O_2C{-}R)_3]^-$ U−O_{yl} and equatorial U−O bond lengths (Table S2) are comparable to those of crystalline mononuclear hexagonal-bipyramidal uranyl carboxylate complexes: i.e., 1.78 and 2.47 Å, respectively.[58] For plutonyl, the GS isomers are pentacoordinated, with the hexacoordinated isomer being higher in energy: i.e., by 29 kJ mol^{-1} for $[PuO_2(O_2C{-}CCCH_3)_3]^-$ at the B3LYP/TZ level. The optimized structures of the $[An^{VI}O_2(O_2C{-}R)_3]^-$ (R = C_6H_5, C_6F_5, CH_3CC) ground-state ions are shown in Figure S3 in the Supporting Information. The $[O_2C{-}C_6H_5]^-$ ligands in $[UO_2(O_2C{-}C_6H_5)_3]^-$ lie on the equatorial plane, whereas the increased repulsion between the oxygen and the fluorine atoms in $[UO_2(O_2C{-}C_6F_5)_3]^-$ cause an out-of-plane rotation of the C_6F_5 rings of ca. 45°: i.e., they lie on a plane between the equatorial and axial planes. The total charge donation from the ligands to the central UO_2 unit is higher for R = CH_3 (0.813 e) and decreases in the order CH_3 > CH_3CC > C_6H_5 > C_6F_5 (0.759 e). Substitution of the central uranyl for plutonyl for a given ligand produces in the two studied cases a small increase of ligand electron donation (Table S2). There is generally a good correlation between the ligand charge donation and the U−O_{yl} bond length: higher charge donation induces elongation and weakening of the U−O_{yl} bond, which is also manifested as decreasing uranyl vibrational frequencies.[59] Selected geometrical parameters of the decarboxylation products (Figure 4) are reported in Table S1 in the Supporting Information. The C_6H_5 ring in the GS structure is found to form hydrogen bond interactions with the two O_{yl} atoms; a higher energy structure in which the C_6H_5 ligand lies in the equatorial plane and forms hydrogen bonds with two neighboring $[O_2C{-}C_6H_5]^-$ oxygen atoms was found to be only 2 kJ mol^{-1} higher in energy (B3LYP/TZ). The GS structures for the $[(C_6F_5)AnO_2(O_2C{-}C_6F_5)_2]^-$ complexes (An = U, Pu) contain a C_6F_5 ligand, as well as the two other C_6F_5 rings rotated: i.e., lying on planes that fall between the equatorial and axial planes. Structural isomers close in energy to the $[(CH_3CC)AnO_2(O_2C{-}CCCH_3)_2]^-$ GS structure were identified and are reported in Figure S4 in the Supporting Information for An = U. Isomers of the GS decarboxylation products not containing An−C were also considered; in all cases those structures corresponded to high-energy isomers (i.e., Figure S4, last isomer). In particular, the possibility of a transfer of the decarboxylated R group to the O_{yl} rather than to the An atom to form the An(IV) complex $[(RO)An^{IV}O(O_2C{-}R)_2]^-$ was analyzed for the representative case of R = CH_3 and An = U. The resulting $[(CH_3O)UO(O_2C{-}CH_3)_2]^-$ isomer (B3LYP/TZ) was found to be 73 kJ mol^{-1} higher in energy than the organometallic GS isomer. As a consequence, this alternative decarboxylation mechanism was not further considered. The bonding properties of the decarboxylation products are discussed in detail below.

Decarboxylation: Comparison between Experiment and Theory. The energetics in Table 2 for the dissociation reactions of uranyl complexes shows that for all four ligands the decarboxylation reaction (eq 1) is the most favorable thermodynamically (least endothermic), followed by the elimination of an anion ligand, which produces a neutral $[U^{VI}O_2(O_2C{-}R)_2]$ complex (eq 2), with the process involving reduction of the $U^{VI}O_2$ moiety (eq 3) being the most energetically unfavorable (degenerate in energy with eq 2 for R = CH_3CC). For R = CH_3, C_6F_5, CH_3CC, neutral and anion ligand loss from $[U^{VI}O_2(O_2C{-}R)_3]^-$ are computed to be energetically similar, to within <30 kJ mol^{-1}, with the latter being slightly lower in energy. Anion ligand loss cannot be experimentally excluded, but it is apparent that neutral ligand loss is a significant channel despite the fact that it is energetically slightly less favorable. It may be that there is a barrier to anion ligand loss because the negative charge needs to be localized on a single ligand prior to elimination. For R = C_6H_5, anion ligand loss is computed to be much lower in energy, by 106 kJ mol^{-1}. Although the $[O_2C{-}C_6H_5]^-$ anion is below the low-mass CID cutoff, it is possible to evaluate the contribution of anion ligand loss. When undetected anion loss is significant, the total ion intensity decreases upon CID to a greater extent than the decrease due to typical ion loss upon manipulation. The measured decrease in ion intensity was found to be relatively minor (see Figure S8 in the Supporting Information), indicating that the loss of neutral ligand was dominant over loss of anionic $[O_2C{-}C_6H_5]^-$, despite the fact that the latter is energetically less demanding by more than 100 kJ mol^{-1}. This result suggests a substantial barrier for loss of $[O_2C{-}C_6H_5]^-$.

The decarboxylation process is expected to involve a kinetic barrier associated with ligand rearrangement necessary to enable the elimination of CO_2. In contrast, neutral ligand elimination is not expected to have a significant barrier in excess of the net endothermicity. As remarked above, the results suggest that there may be a barrier to anion ligand loss. A comparison between different ligands (Table 2) shows that the most facile decarboxylation process occurs for the $[O_2C{-}C_6F_5]^-$ (65 kJ mol^{-1}) and $[O_2C{-}CCCH_3]^-$ (80 kJ mol^{-1}) ligands, which is in accord with the experimentally observed dominance of decarboxylation (Figure 2 and Figure S2 in the Supporting Information) for these ligands. The other two studied decarboxylation reactions (R = CH_3, C_6H_5) have endothermicities comparable to one another (150 and 160 kJ mol^{-1}, respectively), which are considerably higher than the energies for R = CH_3CC, C_6F_5. A similar ease of decarboxylation has been previously noted for the formation of organomagnesates: i.e., R = CH_3CC (the easiest) in comparison to the more endothermic R = C_6H_5, CH_3, which show comparable energetic requirements for decarboxylation.[21,60] Despite the fact that for R = CH_3, C_6H_5 decarboxylation is lower in energy than neutral ligand loss (eq 3) by more than 100 kJ mol^{-1}, the overwhelmingly dominant pathway is the more endothermic ligand loss process, presumably due to energy barriers associated with CO_2 loss. On the basis of these results it appears that under these CID conditions decarboxylation must be endothermic by less than ca. 100 kJ mol^{-1} to appreciably compete with ligand loss. Threshold CID experiments were also performed to further test the relative ease of decarboxylation trends predicted by the

DOI: 10.1021/acs.organomet.6b00079
Organometallics 2016, 35, 1228−1240

computational calculations. Colorado and Brodbelt have demonstrated the use of critical energies for threshold CID in a QIT to evaluate relative dissociation energies.[61] Although the instrument employed for the present studies is not well-suited to quantify the CID energy parameter, it is possible to increase the nominal CID "voltage" and monitor the onset of fragmentation processes. Energy-dependent CID was performed on $[UO_2(O_2C{-}R)_3]^-$ for R = CH_3CC, CH_3, with the results being shown in Figures S5 and S6 in the Supporting Information, respectively. These two complexes were selected to test the utility of the approach because they exhibited the greatest disparity in fixed relatively high energy decarboxylation yields (Table 1), which reflect the large difference in computed decarboxylation energies (Table 2). Furthermore, the masses (m/z) of these two complexes, 519 and 447, are sufficiently similar that excitation and trapping differences should be minimized for the same instrumental parameters. The threshold CID energy is defined here as the energy for which fragmentation becomes apparent and continuously increases for higher CID energies; it is not practical to employ a value such as 10% fragmentation because for R = CH_3 the decarboxylation channel never reaches this contribution due to overwhelmingly dominant ligand loss. When the nominal CID voltage was increased in 0.01 V increments, the decarboxylation onset was identified as 0.19 V for R = CH_3CC and 0.24 V for R = CH_3, both with a resolution of ±0.01 V. The results are in accord with the computed decarboxylation energies, 80 kJ mol^{-1} for R = CH_3CC and 150 kJ mol^{-1} for R = CH_3, but demonstrate the energy resolution limitations of this approach for these systems with this instrument: a difference in fragmentation energy of 70 kJ mol^{-1} results in a change in threshold nominal CID energy of only 0.05 ± 0.02 V. Comparison of the threshold energies for decarboxylation (eq 1) and reduction (eq 3) for R = CH_3 further reveals the limitation of this approach for these systems under these conditions. For R = CH_3, eq 3 is computed to be 113 kJ mol^{-1} more endothermic than eq 1, but it is the dominant CID pathway presumably due to kinetic barriers for decarboxylation. For R = CH_3 the CID threshold for eq 1 is 0.24 V and that for eq 3 is 0.23 V; the values are nearly identical to within the experimental resolution despite the large difference in exothermicity and the overwhelming dominance of eq 3 at higher energies. Unsurprisingly, the threshold CID energies appear to be determined by dissociation kinetics rather than thermodynamics for a process such as decarboxylation, which requires substantial rearrangement during fragmentation.

The $[PuO_2(O_2C{-}R)_3]^-$ decarboxylation processes (eq 1) that were studied computationally (for R = CH_3, CH_3CC) have reaction energetics significantly (ca. 30−60 kJ mol^{-1}) lower than those of the uranyl analogues. Most notably, the neutral ligand losses that involve reduction of the metal center (eq 3) are much lower in energy for Pu and in the two studied cases are almost degenerate in energy with decarboxylation (within 13 kJ mol^{-1}). This result is in accord with the comparative reduction potentials for $U^{VI}O_2^{2+}/U^{V}O_2^{+}$ and $Pu^{VI}O_2^{2+}/Pu^{V}O_2^{+}$: +0.09 and +0.94 V, respectively.[4] On the basis of the near energetic degeneracy and the presumed necessity to surmount barriers during decarboxylation, it would be expected that ligand loss should dominate for both of the studied $[PuO_2(O_2C{-}R)_3]^-$ species; this is the case for R = CH_3 but not for R = CH_3CC. For $[PuO_2(O_2C{-}CCCH_3)_3]^-$, decarboxylation (eq 1) is computed to be only ca. 8 kJ mol^{-1} lower in energy than ligand loss (eq 3). In view of the presumed necessity for substantial rearrangement barriers for CO_2 elimination, as was invoked above to explain the results for uranium complexes, it would be expected that ligand loss should dominate. Surprisingly, decarboxylation is dominant, with no ligand loss observed. This result suggests that the barriers, and thus the mechanism, for decarboxylation are not necessarily similar for all of the ligands. In particular, the dominance of decarboxylation for $[PuO_2(O_2C{-}CCCH_3)_3]^-$ suggests a distinctive mechanism with this ligand that does not require surmounting significant energy barriers. It should be noted that for $[(CH_3CC)UO_2(O_2C{-}CCCH_3)_2]^-$ (Figure S4 in the Supporting Information) there are three low-lying organometallic isomers within 12 kJ mol^{-1}: two with end-on U−C bonds and one with a side-on orientation having η^2 coordination to form a three-membered metallacycle. It may be that the distinctive binding nature of the CH_3CC ligand enables an alternative lower-energy decarboxylation mechanism.

Hydrolysis of $[(R)AnO_2(O_2C{-}R)_2]^-$. Exposure of the $[(R)AnO_2(O_2C{-}R)_2]^-$ organoactinyl complexes to background water in the ion trap resulted in spontaneous hydrolysis (eq 5) for all four studied organouranyl complexes, as well as for the accessible neptunyl and plutonyl organoactinyl complexes $[(CH_3CC)AnO_2(O_2C{-}CCCH_3)_2]^-$ and $[(C_6F_5)AnO_2(O_2C{-}C_6F_5)_2]^-$ (An = Np, Pu).

$$[(R)AnO_2(O_2C{-}R)_2]^- + H_2O \rightarrow [(OH)AnO_2(O_2C{-}R)_2]^- + HR \quad (5)$$

The relative hydrolysis rates normalized to the same (unknown; ca. 10^{-6} Torr) water pressure are summarized in Table 3; an example of the derivations of these rates is given in the Supporting Information. Comparative hydrolysis rates for $[(CH_3CC)AnO_2(O_2C{-}CCCH_3)_2]^-$ (An = U, Np, Pu) are illustrated in Figure 5. A similar comparison for $[(C_6F_5)AnO_2(O_2C{-}C_6F_5)_2]^-$ is reported in Figure S7 in the Supporting Information. As the rates in Table 3 indicate, it is apparent that hydrolysis is most facile for An = U and least so for An = Pu. The results in Table 3 for $[(R)UO_2(O_2C{-}R)_2]^-$ reveal the following relative hydrolysis rates for the four studied R: $CH_3CC \gg CH_3 > C_6H_5 > C_6F_5$ (Figure S9 in the Supporting Information). The results for the organoactinyls where An = Np, Pu show the same rate relationship for the two ligands: $CH_3CC \gg C_6F_5$ (Figure S10 in the Supporting Information). The substantial differences in hydrolysis rates, for different An and for different organic ligands, suggest that gas-phase hydrolysis of organoactinyls provides an indication as to the inherent stabilities of these complexes and specifically of the An−C bonds. The differences apparent in Table 3 are assessed below by computational evaluations of selected hydrolysis processes.

Table 3. Hydrolysis Rates (s^{-1}) for $[(R)AnO_2(O_2C{-}R)_2]^-$ Normalized to the Same $P[H_2O]$ for An = U, Np, Pu and R = CH_3, C_6H_5, C_6F_5, CH_3CC[a]

	CH_3	C_6H_5	C_6F_5	CH_3CC
U	0.073	0.034	0.015	0.62
Np	n/a	n/a	0.0024	0.29
Pu	n/a	n/a	0.0006[b]	0.11

[a]The estimated precision is ±10%. [b]The estimated precision is ±50%.

DOI: 10.1021/acs.organomet.6b00079
Organometallics 2016, 35, 1228−1240

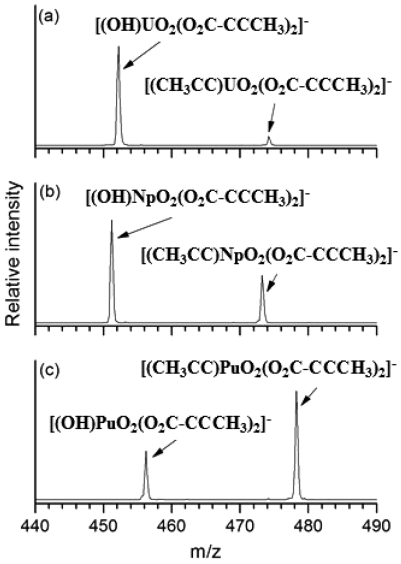

Figure 5. Mass spectra after reaction of $[(CH_3CC)AnO_2(O_2C{-}CCCH_3)_2]^-$ with the same background water pressure for 4 s: (a) An = U; (b) An = Np; (c) An = Pu.

The abundance of $[(C_6F_5)_2AnO_2(O_2C{-}C_6F_5)]^-$ was sufficient such that the sequential hydrolysis given by eqs 6 and 7 could be studied.

$$[(C_6F_5)_2AnO_2(O_2C{-}C_6F_5)]^- + H_2O \rightarrow [(C_6F_5)(OH)AnO_2(O_2C{-}C_6F_5)]^- + HC_6F_5 \quad (6)$$

$$[(C_6F_5)(OH)AnO_2(O_2C{-}C_6F_5)]^- + H_2O \rightarrow [(OH)_2AnO_2(O_2C{-}C_6F_5)]^- + HC_6F_5 \quad (7)$$

The results are shown in Figure S11 in the Supporting Information as the time-dependent decay of $[(C_6F_5)_2AnO_2(O_2C{-}C_6F_5)]^-$ and simultaneous ingrowth of the first and second hydrolysis products; these abundance relationships are characteristic of two sequential reactions, eqs 6 and 7. The abundance of the second hydrolysis product begins to exceed that of the first at ca. 0.7 s for U, at ca. 1.5 s for Np, and at ca. 3 s for Pu, revealing an overall reactivity order the same as that for hydrolysis of $[(C_6F_5)AnO_2(O_2C{-}C_6F_5)_2]^-$: U > Np > Pu. A particularly notable result of the hydrolysis experiments is that U−C bonds are the most susceptible to hydrolysis and Pu−C bonds are the least susceptible.

Computed Hydrolysis of $[(R)An(O_2C{-}R)_2]^-$: Comparison with Experiment. The computed hydrolysis energies are summarized in Table 4; geometrical parameters of all the studied hydroxide products are included in Table S5 in the Supporting Information. All of the studied hydrolysis reactions are exothermic, with a general slight decrease in exothermicity upon going from the uranyl to the plutonyl complexes for the two computed ligands, which parallels the decrease in the hydrolysis reaction rates observed for R = C_6F_5, CH_3CC upon going from U to Pu (Table 3). For a given ligand the U−C bonds are most susceptible to hydrolysis and the Pu−C bonds the least, as assessed both by experimental results and by the computed energetics. For $[(R)U(O_2C{-}R)_2]^-$, the exothermicity of the hydrolysis reactions is highest for R = CH_3, followed by C_6H_5, CH_3CC, and C_6F_5. A comparison between these results and the measured hydrolysis rates shows a correlation between the exothermicity of the reaction in the series CH_3, C_6H_5, and C_6F_5: the more exothermic, the faster the hydrolysis. However, the notably higher hydrolysis rates observed in the case of CH_3CC cannot be explained on the basis of the computed reaction energetics. As observed for decarboxylation, it would seem that the CH_3CC moiety enables a reaction mechanism that results in much more efficient hydrolysis than would be predicted on the basis of thermodynamics alone.

Table 4. Computed Hydrolysis Energies ($\Delta E°_{hyd}$) for Selected $[(R)An(O_2C{-}R)_2]^-$ [a]

	CH_3	C_6H_5	C_6F_5	CH_3CC
U	−170	−149	−82	−97
Np	n/a	n/a	−79	−96
Pu	n/a	n/a	−71	−92

[a] In kJ mol^{-1}, obtained at the B3LYP/TZ level of theory. The identity of R is at the top of each column.

Although a complete analysis of the hydrolysis reaction mechanisms for the different ligands studied here is beyond the scope of this work, a preliminary study of the reaction mechanism for the relatively simple system comprised of acetate and methyl ligands bound to uranyl was performed. To assess the influence of the actinide atom, this study was extended to hydrolysis of $[(CH_3)NpO_2(O_2C{-}CH_3)_2]^-$. We underscore that $[(CH_3)NpO_2(O_2C{-}CH_3)_2]^-$ was not observed experimentally, but is considered here solely to analyze the effect on the mechanism of the actinide center for the least computationally demanding example, the acetate ligand. The obtained results are illustrated in Figures 6 and 7. A number of $[(CH_3)AnO_2(O_2C{-}CH_3)_2]{-}(H_2O)^-$ inner- and outer-sphere complexes close in energy and with equatorial coordination numbers between 4 and 6 were identified. The lowest-energy structure has a coordination number of 4 and contains an inner-sphere water and two monocoordinated acetate ions, which interact via hydrogen bonds with the water molecule located in a trans position with respect to the methyl ligand. The GS isomer is followed in energy (+14 kJ mol^{-1}) by an isomer containing an outer-sphere water molecule with coordination number 5. The hydrolysis reaction mechanism involves the outer-sphere water−anion complex as the first intermediate (**I**), in which the water molecule interacts by hydrogen bonding with an O_{yl} oxygen atom and with an acetate oxygen atom. The water addition is exothermic by ca. 40 kJ mol^{-1}, which is much less than the ca. 140 kJ mol^{-1} exothermic association of a water molecule with the metal center of cationic AnO_2^+ to create a much stronger $An^{x+}{-}OH_2$ electrostatic bond.[33] The reaction proceeds via the formation of a transition state (**TS**) in which the water molecule is inserted into the inner sphere of the reaction complex, with one of the H atoms retaining a hydrogen bond with an acetate and the other interacting with the CH_3 ligand (Figure 7); in this **TS** the An−O distance is essentially the same, ca. 2.5 Å, as in $AnO_2(H_2O)^+$, indicating a significant An−O bonding interaction. Notably, the energy difference between the first intermediate and the transition state is only 45 kJ mol^{-1} for An = U. Analogous hydrogen atom transfer in $UO_2(H_2O)^+$ to yield $UO(OH)_2^+$ introduces a barrier of ca. 150 kJ mol^{-1}.[62] The relatively low barrier for hydrogen atom transfer in the organometallic complex enables the observed hydrolysis. The exit channel involves the formation of the loosely bound hydroxide−methane intermediate complex **II**, which ultimately eliminates CH_4. The substitution of uranyl by neptunyl results in an increase in the **TS** activation barrier,

DOI: 10.1021/acs.organomet.6b00079
Organometallics 2016, 35, 1228−1240

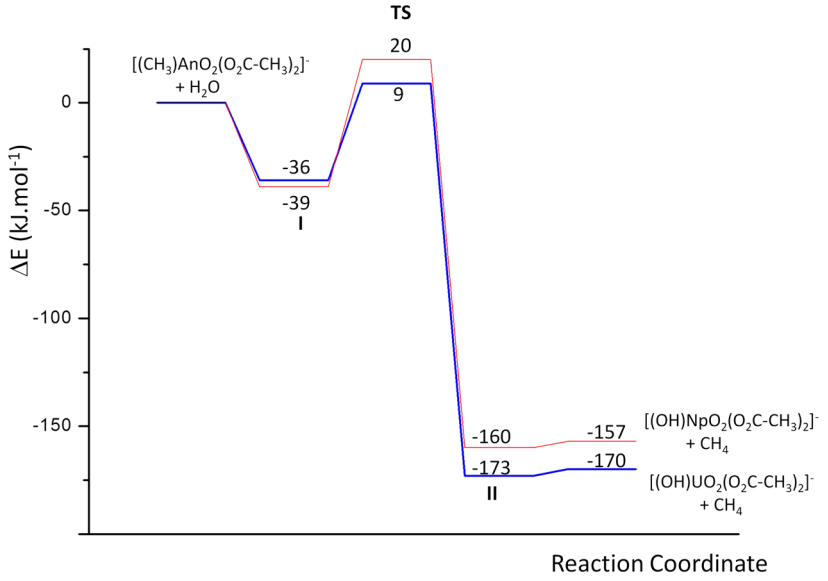

Figure 6. Reaction pathways for the $[(CH_3)AnO_2(O_2C{-}CH_3)_2]^-$ hydrolysis reactions for An = U (blue) and An = Np (red). Energies are relative to the reactants ($E \equiv 0$) in kJ mol^{-1}.

from 9 to 20 kJ mol^{-1} above the reactant energies (Figure 6). We note that the initial and final complexes can be considered as comprised of $[(CH_3)AnO_2]^+$ and $[(OH)AnO_2]^+$ moieties, which consist of hexavalent actinyl cores, AnO_2^{2+}, coordinated by an inner-sphere anion ligand, CH_3^- or OH^-. As for other reactions,[62] the energies of the transition state, intermediate **II**, and products are all shifted to higher energy for neptunyl relative to uranyl, with the result that although the rate-determining barrier is the **TS**, the relative rates correlate with the net reaction exothermicities. Although a similar mechanism and relationship between the **TS** barriers and the hydrolysis energy would be expected for similar ligands R, extrapolation to different types of ligands is not necessarily valid. This is particularly the case for the $[O_2C{-}CCCH_3]^-$ ligand, for which a number of low-energy decarboxylation product isomers were identified (Figure S4 in the Supporting Information). Alternative lower-energy pathways introduced by the accessibility of other structures could account for the more facile hydrolysis of the $[(CH_3CC)(AnO_2)(O_2C{-}CCCH_3)_2]^-$ complexes. The decreasing hydrolysis exothermicity, minor but consistent, from U to Np to Pu is intriguing. In essence, it is evidently more favorable to convert an An−C to an An−O(H) bond for An = U than for An = Pu, with the case of An = Np being intermediate.

IRMPD of Selected Uranyl Complexes. The observed and computed IR spectra for the decarboxylation products $[(CH_3CC)UO_2(O_2C{-}CCCH_3)_2]^-$ and $[(C_6F_5)UO_2(O_2C{-}C_6F_5)_2]^-$ are shown in Figures 8 and 9. The anions were isolated and photofragmented using FELIX to generate IRMPD spectra, covering the region from 1300 to 2100 cm^{-1} in the case of $[(CH_3CC)UO_2(O_2C{-}CCCH_3)_2]^-$ and from 700 to 1650 cm^{-1} for $[(C_6F_5)UO_2(O_2C{-}C_6F_5)_2]^-$. A uniform scaling factor of 0.97 was applied to all harmonic B3LYP/TZ frequencies to account for mode anharmonicities.[63−65] The overall correspondence between calculated and experimental band positions is good; all observed bands in the IR spectra are assignable to bands predicted at the B3LYP level. In particular, the $[(CH_3CC)UO_2(O_2C{-}CCCH_3)_2]^-$ spectrum shows four distinctive bands: two intense bands at ca. 1420 and 1560 cm^{-1} that are associated with the C−CO_2 stretching and the asymmetric O−C−O stretching modes, respectively, and two less intense bands at ca. 1680 and 2070 cm^{-1}. The band at ca. 2070 cm^{-1} corresponds to the decarboxylated ligand C≡C triple bond stretching mode ($d_{C\equiv C}$ = 1.225 Å). According to computations, the C≡C bond stretching mode for the butynoate ligands ($d_{C\equiv C}$ = 1.205 Å) is found at higher frequencies: i.e., 2268 cm^{-1}. It is worth mentioning that this frequency, as well as the C≡C bond distance ($d_{C\equiv C}$ = 1.225 Å), remains unchanged for the corresponding neptunyl and plutonyl isomers, which points out the highly ionic nature of the interaction between the actinyl ions and the CH_3CC ligand (Table S3 in the Supporting Information). This band at high energies is, as expected, absent in the $[(OH)UO_2(O_2C{-}CCCH_3)_2]^-$ hydrolysis product (Figure S12 in the Supporting Information). In Figure 8, in addition to the GS computed frequencies, the corresponding frequencies for a low-energy tetracoordinated isomer (at +15 kJ mol^{-1}, see Figure S4 in the Supporting Information) are shown; the presence of a peak at ca. 1680 cm^{-1} is characteristic of an asymmetric O−C−O stretching mode of a monodentate ligand. Variable denticities of carboxylate ligands to different metallic centers have been previously reported;[15,66] uranyl complexes having variable denticity have been reported by Groenewold and collaborators.[67]

The peak at ca. 2070 cm^{-1} reveals the presence of isomers containing a C atom involved in a triple bond and interacting with the metal atom, i.e. the CH_3CC ligand present in the GS structure and in the tetracoordinated isomer at 15 kJ mol^{-1}, whereas the absence of peaks between 1950 and 2000 cm^{-1} indicates that the isomers at 11 and 12 kJ mol^{-1} above the GS are not present (Figures S4 and S14 in the Supporting Information). The absence of these low-energy isomers may be due to activation energies needed for ligand rearrangement. Decarboxylation products $[(R)UO_2(O_2C{-}R)_2]^-$, as well as their corresponding hydrolysis products, $[(OH)UO_2(O_2C{-}R)_2]^-$ (for which partial IR spectra were recorded; see Figure S12 in the Supporting Information), with coordination 4 instead of 5, namely, containing a bidentate and a monodentate $[O_2C{-}R]$ ligand, were generally found to be between 14 and 20 kJ mol^{-1} higher in energy than the corresponding

DOI: 10.1021/acs.organomet.6b00079
Organometallics 2016, 35, 1228−1240

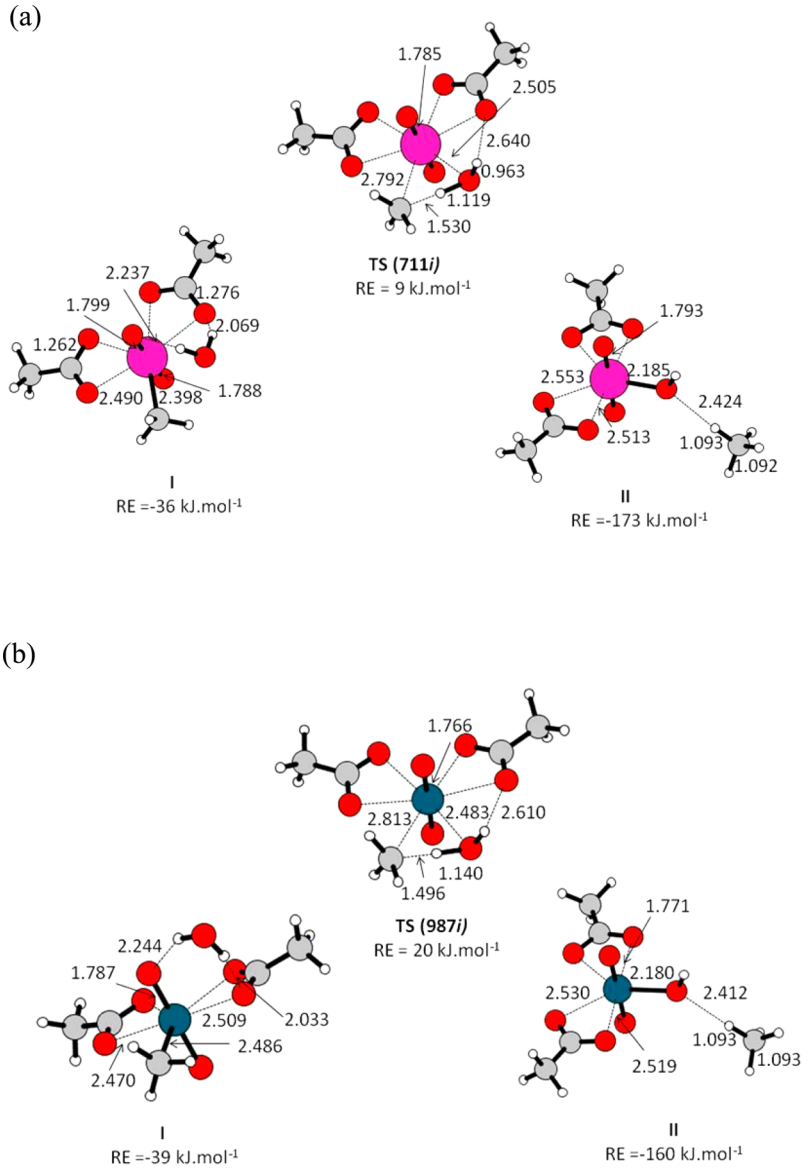

Figure 7. Optimized geometrical parameters of species involved in hydrolysis reaction pathways shown in Figure 6 for (a) $[(CH_3)UO_2(O_2C{-}CH_3)_2]^-$ and (b) $[(CH_3)NpO_2(O_2C{-}CH_3)_2]^-$. Energies are relative to the reactants (RE). The imaginary frequencies characterizing the transition states (TS) are given in parentheses.

pentacoordinated GS structure. The two intense peaks are at 1420 and 1560 cm^{-1}, which correspond to vibrations associated with the carboxylate ligands, are present in all the studied isomers.

A good correspondence between the observed and computed bands of the $[(C_6F_5)UO_2(O_2C{-}C_6F_5)_2]^-$ GS structure is evident in Figure 9. The band at ca. 780 cm^{-1} is due to the CO_2 scissoring modes of the $[O_2C{-}C_6F_5]^-$ ligands. The bands in the region of 900−1100 cm^{-1} correspond mostly to the benzene ring deformation modes; the asymmetric O−U−O stretching mode was computed to be at 937 cm^{-1}. The bands in the region of 1400−1450 cm^{-1} are assigned to aromatic C−C stretches, and the band at ca. 1600 cm^{-1} is ascribed to the asymmetric O−C−O stretching mode of bidentate $[O_2C{-}C_6F_5]^-$ ligands. It is worthwhile to compare these frequencies with those reported by Deacon et al. for a series of dioxobis(pentafluorobenzoato) uranium(VI) complexes.[16] The asymmetric O−C−O stretching mode was 1562 cm^{-1} for $UO_2(O_2C{-}C_6F_5)$ and 1580−1558 cm^{-1} for $UO_2(O_2C{-}C_6F_5)$bpy (bpy = 2,2′-bipyridyl), whereas the asymmetric O−U−O stretching modes for the same complexes were determined to be 948 and 932 cm^{-1}, respectively.[16] The presence of a tetracoordinated isomer, which was computed to be 18 kJ mol^{-1} higher in energy than the GS, is not obvious in this spectrum. From a comparison of the observed and computed spectra for the precursor $[UO_2(O_2C{-}C_6F_5)_3]^-$ ion it is concluded that, in addition to the GS hexacoordinated ion, there is also present a pentacoordinated isomer (Figure S13 in the Supporting Information). The presence of a monodentate $[O_2C{-}C_6F_5]^-$ ligand is established by the appearance of peaks in the region of 1250−1350 cm^{-1}, which are associated with the C−CO_2 stretching mode, and by the shift of the asymmetric O−C−O stretching mode to higher energies (ca. 1690 cm^{-1}). These peaks are absent in the $[(C_6F_5)UO_2(O_2C{-}C_6F_5)_2]^-$ spectrum for the decarboxylation product.

DOI: 10.1021/acs.organomet.6b00079
Organometallics 2016, 35, 1228−1240

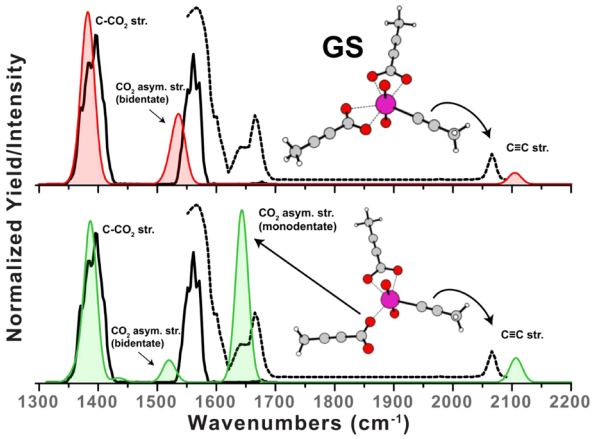

Figure 8. IRMPD spectra of $[(CH_3CC)UO_2(O_2C{-}CCCH_3)_2]^-$ (black). The spectrum indicated by a dashed line was acquired at a higher photon flux. (top) Comparison with the computed spectrum for the $[(CH_3CC)UO_2(O_2C{-}CCCH_3)_2]^-$ ground-state (GS) isomer. (bottom) Comparison with the computed spectrum for the tetracoordinated isomer, computed to be 15 kJ mol^{-1} higher in energy than the GS. The spectra indicate the presence of both the pentacoordinated GS and low-energy tetracoordinated isomer. Harmonic frequencies computed at the B3LYP/TZ method were scaled by a factor of 0.97 and convoluted with a 25 cm^{-1} Gaussian line shape function. The computed intensities were normalized to the most intense experimental peak.

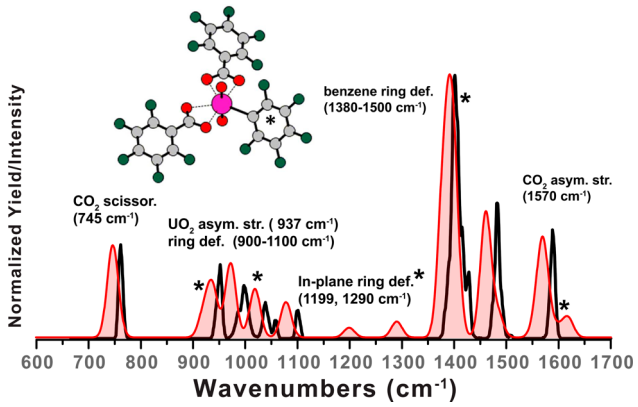

Figure 9. IRMPD spectrum of $[(C_6F_5)UO_2(O_2C{-}C_6F_5)_2]^-$ (black). Harmonic frequencies corresponding to the $[(C_6F_5)UO_2(O_2C{-}C_6F_5)_2]^-$ GS isomer were computed at the B3LYP/TZ method, scaled by a factor of 0.97 and convoluted with a 25 cm^{-1} Gaussian line shape function (red). The computed intensities were normalized to the most intense experimental peak. The computed bands marked with an asterisk correspond to vibrational modes associated with the decarboxylated perfluorophenyl ligand.

CONCLUSIONS

The fragmentation chemistry of $[AnO_2(O_2C{-}R)_3]^-$ ions was investigated in the gas phase using quadrupole ion trap mass spectrometry for a series of carboxylate ligands and An = U, Np, Pu. Decarboxylation products $[(R)AnO_2(O_2C{-}R)_2]^-$, which comprise discrete U−C organouranyl bonds, were detected for the four studied $[O_2C{-}R]^-$ ligands, R = CH_3, C_6H_5, C_6F_5, CH_3CC. In contrast, only $[(CH_3CC)AnO_2(O_2C{-}CCCH_3)_2]^-$ and $[(C_6F_5)AnO_2(O_2C{-}C_6H_5)_2]^-$ were detected for neptunyl and plutonyl. To the best of our knowledge, this is the first report of complexes containing actinide−carbon bonds for neptunyl and plutonyl. Density functional theory calculations indicate that the decarboxylation reaction is thermodynamically more favorable (less endothermic) than ligand loss for all of the studied uranyl complexes. In selected cases, plutonyl homologues were also computationally studied and it was found that ligand loss, with concomitant reduction of the metal center from $Pu^{VI}O_2$ to $Pu^{V}O_2$, is energetically competitive with decarboxylation; this, in contrast to the corresponding uranyl reactions, is attributed to the lower U(VI)/U(V) reduction potential, which stabilizes the hexavalent oxidation state of uranium.

IRMPD spectra acquired for selected anion complexes are in good agreement with computed spectra. The presence of both bidentate and monodentate coordinated carboxylate ligands was revealed. A particularly significant result was the appearance of a peak at ca. 2070 cm^{-1} for $[(CH_3CC)UO_2(O_2C{-}CCCH_3)_2]^-$. This peak corresponds to a triple C≡C bond stretching mode characteristic of the computed lowest-energy organouranyl structure that comprises a U−C≡C−CH_3 bonding motif, thereby providing evidence for a discrete uranium−carbon bond.

The intrinsic stability of the organoactinyl bonds was investigated by measuring the relative hydrolysis rates across the series U, Np, and Pu. The hydrolysis rates generally diminish upon going from U to Pu, which parallels the computed decrease in exothermicity of hydrolysis from U to Pu. The hydrolysis mechanism was computed for the relatively tractable cases of $[(CH_3)AnO_2(O_2C{-}CH_3)_2]^-$ (An = U, Np). The mechanism was found to proceed by formation of an outer-sphere hydrate; the water molecule then inserts into the inner sphere concomitant with H atom transfer to the CH_3 group to produce the hydroxide and CH_4. The transition state barrier for An = Np is higher than that for An = U, in accord with generally slower hydrolysis of the neptunyl complexes. The higher **TS** for An = Np correlates with a lower exothermicity, which indicates that conversion of an An−C to an An−O bond is less favorable for An = Np than for An = U and even less favorable for An = Pu. The results suggest that the stabilities of organoactinyls toward hydrolysis should increase across the series from uranyl to neptunyl to plutonyl. The chemical properties of the An−C bonds were further analyzed by QTAIM. The results suggest that the bonds are largely ionic, similar to the case for An−O(H) hydroxyl bonds, though with significant covalent character.

ASSOCIATED CONTENT

Supporting Information

The Supporting Information is available free of charge on the ACS Publications website at DOI: 10.1021/acs.organomet.6b00079.

Details of QTAIM bond analysis, geometrical parameters and QTAIM properties of $[An^{VI}O_2(O_2C{-}R)_3]^-$ and $[(OH)An^{VI}O_2(O_2C{-}R)_2]^-$ complexes, geometrical parameters of $[An^{V}O_2(O_2C{-}R)_2]^-$ and $[An^{VI}O_2(O_2C{-}R)_2]$ complexes, $[AnO_2(O_2C{-}R)_3]^-$ CID mass spectra for R = C_6H_5, C_6F_5, $[UO_2(O_2C{-}R)_3]^-$ GS geometrical structures, higher-energy $[(CCCH_3)AnO_2(O_2C{-}CCCH_3)_2]^-$ isomers, mass spectra after reaction of $[(C_6F_5)AnO_2(O_2C{-}C_6F_5)_2]^-$ with water, plots of comparative hydrolysis rates for $[(R)UO_2(O_2C{-}R)_2]^-$ (R = CH_3CC, CH_3, C_6H_5, C_6F_5) and $[(R)AnO_2(O_2C{-}R)_2]^-$ (An = U, Np, Pu), IRMPD and computed IR spectra for $[(OH)UO_2(O_2C{-}CCCH_3)_2]^-$, $[UO_2(O_2C{-}$

DOI: 10.1021/acs.organomet.6b00079
Organometallics 2016, 35, 1228−1240

$C_6F_5)_3]^-$, and $[(CH_3CC)AnO_2(O_2C{-}CCCH_3)_2]^-$, kinetics plots for sequential hydrolysis reactions, representative hydrolysis kinetics determination, and energy-dependent CID for $[UO_2(O_2C{-}CCCH_3)_3]^-$ and $[UO_2(O_2C{-}CH_3)_3]^-$ (PDF)
All computed molecule Cartesian coordinates (XYZ)

AUTHOR INFORMATION

Corresponding Authors

*E-mail for M.C.M.: mc.michelini@unical.it.
*E-mail for J.K.G.: jkgibson@lbl.gov.

Notes

The authors declare no competing financial interest.

ACKNOWLEDGMENTS

This work was supported by the U.S. Department of Energy, Office of Basic Energy Sciences, Division of Chemical Sciences, Geosciences, and Biosciences, Heavy Element Chemistry program, at LBNL under Contract No. DE-AC02-05CH11231 (P.D.D., D.R., Y.G., D.K.S., J.K.G.) and by the Office of Science, Office of Workforce Development for Teachers and Scientists (WDTS), under the Science Undergraduate Laboratory Internship (SULI) program (M.M.), by the Università della Calabria, Italy (M.C.M.), by the Fundação para a Ciência e a Tecnologia through project UID/Multi/04349/2013 (J.M.), by start-up funds from the Bayer School of Natural and Environmental Sciences and Duquesne University (M.J.V.S., T.A.C.), and by The Netherlands Organisation for Scientific Research (NWO) under vici-grant no. 724.011.002 and the Stichting Physica (J.O.). This research used resources of the National Energy Research Scientific Computing Center (NERSC), which is supported by the Office of Science of the U.S. Department of Energy under Contract No. DE-AC02-05CH11231.

REFERENCES

(1) Seyferth, D. *Organometallics* **2004**, *23*, 3562−3583.
(2) Reynolds, L. T.; Wilkinson, G. J. *J. Inorg. Nucl. Chem.* **1956**, *2*, 246−253.
(3) Streitwieser, A., Jr.; Müller-Westerhoff, U. *J. Am. Chem. Soc.* **1968**, *90*, 7364−7364.
(4) Edelstein, N. M.; Fuger, J.; Katz, J. J.; Morss, L. R. *The Chemistry of the Actinide and Transactinide Elements*, 3rd ed.; Springer: Dordrecht, The Netherlands, 2006; Vol. *3*, p 1779.
(5) Cornet, S. M.; May, I.; Sarsfield, M. J.; Kaltsoyannis, N.; Haller, J.; Den Auwer, C.; Meyer, D. *J. Alloys Compd.* **2007**, *444-445*, 453−456.
(6) Baker, R. J. *Chem. - Eur. J.* **2012**, *18*, 16258−16271.
(7) Johnson, S. A.; Bart, S. C. *Dalton Trans.* **2015**, *44*, 7710−7726.
(8) Sarsfield, M. J.; Helliwell, M.; Collison, D. *Chem. Commun.* **2002**, 2264−2265.
(9) Sarsfield, M. J.; Steele, H.; Helliwell, M.; Teat, S. J. *Dalton Trans.* **2003**, 3443−3449.
(10) Tourneux, J. C.; Berthet, J. C.; Cantat, T.; Thuery, P.; Mezailles, N.; Ephritikhine, M. *J. Am. Chem. Soc.* **2011**, *133*, 6162−6165.
(11) Schettini, M. F.; Wu, G.; Hayton, T. W. *Chem. Commun.* **2012**, *48*, 1484−1486.
(12) Arnold, P. L.; Casely, I. J.; Turner, Z. R.; Carmichael, C. D. *Chem. - Eur. J.* **2008**, *14*, 10415−10422.
(13) Seaman, L. A.; Hrobarik, P.; Schettini, M. F.; Fortier, S.; Kaupp, M.; Hayton, T. W. *Angew. Chem., Int. Ed.* **2013**, *52*, 3259−3263.
(14) Maynadié, J.; Berthet, J. C.; Thuery, P.; Ephritikhine, M. *Chem. Commun.* **2007**, 486−488.
(15) Connett, J. E.; Davies, A. G.; Deacon, G. B.; Green, J. H. S. *J. Chem. Soc. C* **1966**, 106−111.
(16) Deacon, G. B.; Mackinnon, P. I. *Polyhedron* **1985**, *4*, 103−113.
(17) Deacon, G. B.; Faulks, S. J.; Pain, G. N. *Adv. Organomet. Chem.* **1986**, *25*, 237−276.
(18) Wu, J.; Liu, D.; Zhou, J.-G.; Hagelberg, F.; Park, S. S.; Shvartsburg, A. A. *J. Phys. Chem. A* **2007**, *111*, 4748−4758.
(19) Jacob, A. P.; James, P. F.; O'Hair, R. A. J. *Int. J. Mass Spectrom.* **2006**, *255-256*, 45−52.
(20) O'Hair, R. A. J. *Chem. Commun.* **2002**, 20−21.
(21) Khairallah, G. N.; Thum, C. C. L.; Lesage, D.; Tabet, J.-C.; O'Hair, R. A. J. *Organometallics* **2013**, *32*, 2319−2328.
(22) O'Hair, R. A. J.; Vrkic, A. K.; James, P. F. *J. Am. Chem. Soc.* **2004**, *126*, 12173−12183.
(23) Rijs, N. J.; Khairallah, G. N.; Waters, T.; O'Hair, R. A. J. *J. Am. Chem. Soc.* **2008**, *130*, 1069−1079.
(24) Rijs, N. J.; O'Hair, R. A. J. *Organometallics* **2009**, *28*, 2684−2692.
(25) Khairallah, G. N.; Thum, C. C. L.; O'Hair, R. A. J. *Organometallics* **2009**, *28*, 5002−5011.
(26) Leeming, M. G.; Khairallah, G. N.; da Silva, G.; O'Hair, R. A. J. *Organometallics* **2011**, *30*, 4297−4307.
(27) Woolley, M. J.; Khairallah, G. N.; Donnelly, P. S.; O'Hair, R. A. J. *Rapid Commun. Mass Spectrom.* **2011**, *25*, 2083−2088.
(28) Sraj, L. O.; Khairallah, G. N.; da Silva, G.; O'Hair, R. A. J. *Organometallics* **2012**, *31*, 1801−1807.
(29) MacAleese, L.; Maître, P. *Mass Spectrom. Rev.* **2007**, *26*, 583−605.
(30) Gronert, S. *J. Am. Soc. Mass Spectrom.* **1998**, *9*, 845−848.
(31) Rios, D.; Rutkowski, P. X.; Shuh, D. K.; Bray, T. H.; Gibson, J. K.; Van Stipdonk, M. J. *J. Mass Spectrom.* **2011**, *46*, 1247−1254.
(32) Rutkowski, P. X.; Michelini, M. C.; Bray, T. H.; Russo, N.; Marçalo, J.; Gibson, J. K. *Theor. Chem. Acc.* **2011**, *129*, 575−592.
(33) Rios, D.; Michelini, M. C.; Lucena, A. F.; Marçalo, J.; Bray, T. H.; Gibson, J. K. *Inorg. Chem.* **2012**, *51*, 6603−6614.
(34) Gresham, G. L.; Gianotto, A. K.; Harrington, P. D.; Cao, L. B.; Scott, J. R.; Olson, J. E.; Appelhans, A. D.; Van Stipdonk, M. J.; Groenewold, G. S. *J. Phys. Chem. A* **2003**, *107*, 8530−8538.
(35) Chien, W.; Anbalagan, V.; Zandler, M.; Van Stipdonk, M.; Hanna, D.; Gresham, G.; Groenewold, G. *J. Am. Soc. Mass Spectrom.* **2004**, *15*, 777−783.
(36) Oepts, D.; van der Meer, A. F. G.; van Amersfoort, P. W. *Infrared Phys. Technol.* **1995**, *36*, 297−308.
(37) Kempkes, L. J. M.; Martens, J. K. M.; Grzetic, J.; Berden, G.; Oomens, J. *Rapid Commun. Mass Spectrom.* **2016**, *30*, 483−490.
(38) Kuchle, W.; Dolg, M.; Stoll, H.; Preuss, H. *J. Chem. Phys.* **1994**, *100*, 7535−7542.
(39) Cao, X. Y.; Dolg, M.; Stoll, H. *J. Chem. Phys.* **2003**, *118*, 487−496.
(40) Bryantsev, V. S.; de Jong, W. A.; Cossel, K. C.; Diallo, M. S.; Goddard, W. A.; Groenewold, G. S.; Chien, W.; Van Stipdonk, M. J. *J. Phys. Chem. A* **2008**, *112*, 5777−5780.
(41) Schoendorff, G.; Windus, T. L.; de Jong, W. A. *J. Phys. Chem. A* **2009**, *113*, 12525−12531.
(42) de Jong, W. A.; Aprà, E.; Windus, T. L.; Nichols, J. A.; Harrison, R. J.; Gutowski, K. E.; Dixon, D. A. *J. Phys. Chem. A* **2005**, *109*, 11568−11577.
(43) Lee, C. T.; Yang, W. T.; Parr, R. G. *Phys. Rev. B: Condens. Matter Mater. Phys.* **1988**, *37*, 785−789.
(44) Becke, A. D. *J. Chem. Phys.* **1993**, *98*, 5648−5652.
(45) Valiev, M.; Bylaska, E. J.; Govind, N.; Kowalski, K.; Straatsma, T. P.; van Dam, H. J. J.; Wang, D.; Nieplocha, J.; Apra, E.; Windus, T. L.; de Jong, W. A. *Comput. Phys. Commun.* **2010**, *181*, 1477.
(46) Frisch, M. J., et al. *Gaussian 09, Rev. B.01*; Gaussian, Inc., Wallingford, CT, 2009. See the Supporting Information for the full citation.
(47) Fukui, K. *Acc. Chem. Res.* **1981**, *14*, 363−368.
(48) Gonzalez, C.; Schlegel, H. B. *J. Chem. Phys.* **1989**, *90*, 2154−2161.
(49) Gonzalez, C.; Schlegel, H. B. *J. Phys. Chem.* **1990**, *94*, 5523−5527.

DOI: 10.1021/acs.organomet.6b00079
Organometallics 2016, 35, 1228−1240

(50) Bader, R. F. W. *Atoms in Molecules: A Quantum Theory*; Oxford University Press: Oxford, U.K., 1990.
(51) Keith, T. A. *AIMAll (version 13.05.06)*; 2013; aim.tkgristmill.com.
(52) Groenewold, G. S.; Cossel, K. C.; Gresham, G. L.; Gianotto, A. K.; Appelhans, A. D.; Olson, J. E.; Van Stipdonk, M. J.; Chien, W. *J. Am. Chem. Soc.* **2006**, *128*, 3075−3084.
(53) Leavitt, C. M.; Bryantsev, V. S.; de Jong, W. A.; Diallo, M. S.; Goddard, W. A.; Groenewold, G. S.; Van Stipdonk, M. J. *J. Phys. Chem. A* **2009**, *113*, 2350−2358.
(54) Bakac, A.; Espenson, J. H. *Inorg. Chem.* **1995**, *34*, 1730−1735.
(55) Lucena, A. F.; Carretas, J. M.; Marçalo, J.; Michelini, M. C.; Gong, Y.; Gibson, J. K. *J. Phys. Chem. A* **2015**, *119*, 3628−3635.
(56) Dau, P. D.; Gibson, J. K. *J. Phys. Chem. A* **2015**, *119*, 3218−3224.
(57) Schröder, D.; Soldi-Lose, H.; Schwarz, H. *Aust. J. Chem.* **2003**, *56*, 443−451.
(58) Loiseau, T.; Mihalcea, I.; Henry, N.; Volkringer, C. *Coord. Chem. Rev.* **2014**, *266*−*267*, 69−109.
(59) Groenewold, G. S.; Gianotto, A. K.; McIlwain, M. E.; Van Stipdonk, M. J.; Kullman, M.; Moore, D. T.; Polfer, N.; Oomens, J.; Infante, I.; Visscher, L.; Siboulet, B.; de Jong, W. A. *J. Phys. Chem. A* **2008**, *112*, 508−521.
(60) O'Hair, R. A. J.; Rijs, N. J. *Acc. Chem. Res.* **2015**, *48*, 329−340.
(61) Colorado, A.; Brodbelt, J. *J. Am. Soc. Mass Spectrom.* **1996**, *7*, 1116−1125.
(62) Rios, D.; Michelini, M. C.; Lucena, A. F.; Marçalo, J.; Gibson, J. K. *J. Am. Chem. Soc.* **2012**, *134*, 15488−15496.
(63) Banisaukas, J.; Szczepanski, J.; Eyler, J.; Vala, M.; Hirata, S.; Head-Gordon, M.; Oomens, J.; Meijer, G.; von Helden, G. *J. Phys. Chem. A* **2003**, *107*, 782−793.
(64) Merrick, J. P.; Moran, D.; Radom, L. *J. Phys. Chem. A* **2007**, *111*, 11683−11700.
(65) Groenewold, G.; Van Stipdonk, M. J.; Oomens, J.; de Jong, W. A.; Gresham, G.; McIlwain, M. E. *Int. J. Mass Spectrom.* **2010**, *297*, 67−75.
(66) Deacon, G. B.; Phillips, R. J. *Coord. Chem. Rev.* **1980**, *33*, 227−250.
(67) Groenewold, G.; de Jong, W. A.; Oomens, J.; Van Stipdonk, M. *J. Am. Soc. Mass Spectrom.* **2010**, *21*, 719−727.

DOI: 10.1021/acs.organomet.6b00079
Organometallics 2016, 35, 1228−1240